

Few-photon transport via a multimode nonlinear cavity: theory and applications

Yunkai Wang^{1,2,3} and Kejie Fang^{1,3,4,*}

¹*Holonyak Micro and Nanotechnology Laboratory,
University of Illinois at Urbana-Champaign, Urbana, IL 61801 USA*

²*Department of Physics, University of Illinois at Urbana-Champaign, Urbana, IL 61801 USA*

³*Illinois Quantum Information Science and Technology Center,
University of Illinois at Urbana-Champaign, Urbana, IL 61801 USA*

⁴*Department of Electrical and Computer Engineering,
University of Illinois at Urbana-Champaign, Urbana, IL 61801 USA*

Few-photon transport via waveguide-coupled local quantum systems has attracted extensive theoretical and experimental studies. Most of the study has focused on atomic or atomic-like local quantum systems due to their strong light-matter interaction useful for quantum applications. Here, we study few-photon transport via a waveguide-coupled multimode optical cavity with second-order bulk nonlinearity. We develop a Feynman diagram approach and compute the scattering matrix of the one- and two-photon transport. Based on the calculated scattering matrix, we show highly nonclassical photonic effects, including photon blockade and π -conditional phase shift, are achievable in the waveguide-coupled multimode optical cavity system via quantum interference and linear response engineering. Our results might lead to significant applications of quantum photonic circuits in all-optical quantum information processing and quantum network protocols.

I. INTRODUCTION

The architecture of waveguide-coupled local quantum systems enables coupling flying photons with stationary qubits for light-matter interactions. A prime example is the waveguide quantum electrodynamics, with several types of local quantum systems demonstrated successfully, including trapped atoms [1–3], solid state defects [4, 5], and superconducting qubits [6, 7]. This architecture is also relevant to quantum networks where optic fibers link local quantum nodes for routing, storage, and processing of quantum information encoded in individual photons [8]. In parallel, a large body of theoretical work has been carried out to study few-photon transport in the setting of waveguide-coupled local quantum systems [9–14]. Most of the theoretical and experimental work, though, has focused on qubit-like quantum entities, which are sought to provide strong light-matter interactions for quantum information tasks.

Here, we study few-photon transport via a waveguide-coupled multimode optical cavity with second-order bulk nonlinearity. This is a common device setup used for cavity-enhanced parametric nonlinear optical processes including second-harmonic generation and parametric down-conversion [15–22]. However, its property at the few-photon level has not been fully explored, because bulk nonlinearity is generally believed to be insubstantial to impact single photons. We challenge this perspective by investigating the non-parametric few-photon transport and its physical observations. Besides using a systematic method from Ref. [14] to compute the scattering matrix (S -matrix) of few-photon transport, we develop a Feynman diagram approach which provides further physical insight into the obtained S -matrix while

offering mathematical simplicity in its computation. This method is particularly suited for weak nonlinear systems where only leading order Feynman diagrams are of interest. Exploiting the result of the S -matrix, we then study observational effects of few-photon transport via the waveguide-coupled multimode cavity, including photon blockade, conditional phase shift, and non-classical two-mode correlations. Surprisingly, while these effects are commonly believed to be associated with strong light-matter interaction, we find they could become substantial for waveguide-coupled optical cavities with only weak nonlinearity.

These results reveal a general approach for creation and control of few-photon correlations via quantum interference and linear response engineering. The few-photon transport amplitude of waveguide-coupled local quantum systems is a superposition of the interaction-free, i.e., linear, and interaction-mediated amplitudes. When the linear transmission coefficient is comparable to the interaction-mediated amplitude, quantum interference between the two pathways leads to highly nonclassical correlations between the propagating photons. For weak nonlinear systems, this might need a tuned linear transmission which could be achieved, for example, in a one-port waveguide-cavity configuration. However, this approach is distinct from the post-selection method where photon-photon correlations are induced by the measurement. Our result might lead to significant applications in quantum information science using quantum photonic circuits beyond the parametric regime, including quantum nondemolition measurement of photons [23], two-photon quantum logic gates [24], and nonlinearity-assisted entanglement swapping [25].

* kfang3@illinois.edu

II. SCATTERING MATRIX OF FEW-PHOTON TRANSPORT

The system under consideration is a waveguide-coupled trimodal optical cavity made from $\chi^{(2)}$ materials. A typical realization of such an optical cavity is a microring resonator (Fig. 1a) which supports traveling-wave resonances. These resonances couple via the $\chi^{(2)}$

$$H_{\text{eff}} = (\omega_1 - i\frac{\kappa_1}{2})a_1^\dagger a_1 + (\omega_2 - i\frac{\kappa_2}{2})a_2^\dagger a_2 + (\omega_3 - i\frac{\kappa_3}{2})a_3^\dagger a_3 + g(a_1 a_2 a_3^\dagger + a_1^\dagger a_2^\dagger a_3), \quad (1)$$

where ω_j and κ_j are the frequency and photon loss rate of the j -th resonance, respectively, and g is the trimodal coupling coefficient. For simplicity, we define a complex frequency $\alpha_j \equiv \omega_j - i\frac{\kappa_j}{2}$. For the trimodal interaction to be resonantly enhanced, the three modes need to satisfy the frequency-matching condition $\omega_1 + \omega_2 \approx \omega_3$. The cavity photon loss includes both leakage into the waveguide and intrinsic losses due to, for example, material absorption and surface scattering, i.e., $\kappa_j = \kappa_{je} + \kappa_{ji}$, where κ_{je} is the cavity-waveguide coupling rate and κ_{ji} is the intrinsic photon loss rate. Depending on the configuration of the waveguide-cavity coupling, the relation between the states of the outgoing and incoming photons in the waveguide is determined by the input-output formalism [26]. In this paper, we specifically consider the case of a cavity side-coupled to a waveguide unidirectionally—typical for ring resonators—which has the following input-output relation of the operators,

$$a_{\text{out},j}(t) = a_{\text{in},j}(t) - i\sqrt{\kappa_{je}}a_j(t). \quad (2)$$

It turns out such one-port cavity-waveguide configuration is critical for realizing strong quantum correlations between propagating waveguide photons coupled via a weak nonlinear optical cavity. However, the computation method developed here can be straightforwardly generalized to other waveguide-cavity configurations. For the calculation below, we also assume a linear dispersion of the waveguide, which is justified given the linewidth of the cavity, and thus the operation bandwidth of the system, is much smaller than the cavity frequency [27].

The goal of this section is to calculate the scattering matrix (S -matrix) of the one- and two-photon transport via the waveguide-coupled trimodal $\chi^{(2)}$ cavity (Fig. 1b-d). We first use a systematic method from Ref. [14] and apply it to the present case of a multi-mode $\chi^{(2)}$ cavity. We also develop a Feynman diagram approach which provides further physical insight of the photon transport while lessen the computation complexity associated with the non-perturbative method of Ref. [14], especially for weak nonlinear systems.

nonlinearity when frequency-matching and, if necessary, phase-matching conditions are satisfied. Photons couple in and out of these resonances via the waveguide and meanwhile dissipate in other loss channels. In the Heisenberg-Langevin framework, this open quantum system can be modeled by the following effective Hamiltonian ($\hbar = 1$)

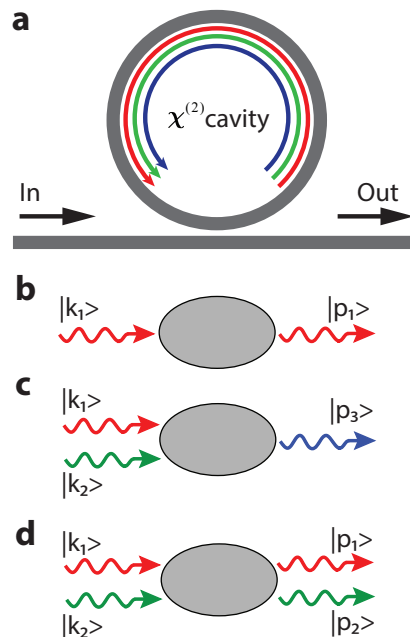


FIG. 1. **a.** A $\chi^{(2)}$ microring cavity with three resonances side-coupled to a waveguide. Red, green, and blue lines corresponds to a_1 , a_2 , and a_3 modes/photons, respectively. **b-d.** Illustrations of few-photon transport processes. $|k\rangle$ denotes the single-photon state with momentum k .

A. One-to-one-photon transport

We first consider the transport of a single photon (Fig. 1b). The amplitude of transport of an incoming photon at time t' to an outgoing photon at time t is given by the time-domain S -matrix

$$S_{t;t'} \equiv \langle 0 | a_{\text{out},1}(t) a_{\text{in},1}^\dagger(t') | 0 \rangle, \quad (3)$$

where the photon is assumed to be in resonant with the a_1 mode. As shown in Ref. [14], the time-domain S -matrix is related to the Green's function of the local system, i.e., here the nonlinear optical cavity, by applying Eq. 2 and

the quantum causality condition

$$[a(t), I(t')] = [a^\dagger(t), I(t')] = 0, \quad \text{for } t \leq t', \quad (4)$$

$$[a(t), O(t')] = [a^\dagger(t), O(t')] = 0, \quad \text{for } t \geq t', \quad (5)$$

where $I(O)(t')$ is a shorthand notation for the input(output) operators that represent either $a_{\text{in(out)}}(t')$ or $a_{\text{in(out)}}^\dagger(t')$. Thus, the single-photon S -matrix becomes

$$S_{t;t'} = \delta(t - t') - \kappa_{1e}G(t; t'), \quad (6)$$

where $G(t; t') = \langle 0 | \hat{T}[a_1(t)a_1^\dagger(t')] | 0 \rangle$ is the two-point Green's function, \hat{T} is the time ordering operator and we have also used $[a_{\text{in(out)}}(t), a_{\text{in(out)}}^\dagger(t')] = \delta(t - t')$ in the derivation.

The Green's function of the local quantum system is calculated using operators time-evolved according to the effective Hamiltonian of 1 [14]. Thus, we proceed

$$\begin{aligned} G(t; t') &= \langle 0 | e^{iH_{\text{eff}}t} a_1 e^{-iH_{\text{eff}}t'} e^{iH_{\text{eff}}t'} a_1^\dagger e^{-iH_{\text{eff}}t'} | 0 \rangle \theta(t - t') \\ &= e^{i\alpha_1(t' - t)} \theta(t - t'), \end{aligned} \quad (7)$$

where $\theta(t - t')$ is the Heaviside step function.

The frequency-domain S -matrix quantifying the transport amplitude between output and input photons with fixed frequency or momentum is given by the Fourier transform of the time-domain S -matrix. For the single-

photon transport,

$$\begin{aligned} S_{p_1; k_1} &\equiv \mathcal{F} \{S_{t;t'}\} \\ &= \int \frac{dt}{\sqrt{2\pi}} e^{ip_1 t} \int \frac{dt'}{\sqrt{2\pi}} e^{ik_1 t'} S_{t;t'} \\ &= \delta(p_1 - k_1) - \kappa_{1e}G(p_1; k_1), \end{aligned} \quad (8)$$

where $G(p_1; k_1)$ is the Fourier transform of the Green's function of 7. This definition of Fourier transform leads to $\langle k|k' \rangle = \delta(k - k')$ given $\langle t|t' \rangle = \delta(t - t')$, where $|k \rangle \equiv \mathcal{F} \{|t \rangle\}$. The momentum-space Green's function thus is

$$G(p_1; k_1) = \frac{i}{k_1 - \alpha_1} \delta(p_1 - k_1). \quad (9)$$

As a result, we have

$$S_{p_1; k_1} = \left[1 - \frac{i\kappa_{1e}}{k_1 - \alpha_1} \right] \delta(p_1 - k_1) \equiv t_{k_1} \delta(p_1 - k_1), \quad (10)$$

where t_{k_1} is the single-photon transmission coefficient. The derivation above straightforwardly applies to transport of a single photon in resonant with other resonances. For the rest of the paper, we use the subscript j in the momentum to indicate photons in resonant with the j -th resonance.

B. Two-to-one-photon transport and vice versa

Next, we consider the transport of two a_1 and a_2 photons to one a_3 photon enabled by the $\chi^{(2)}$ cavity (Fig. 1c). This corresponds to the sum-of-frequency process in nonlinear optics. Following a similar procedure, the time-domain S -matrix of this process is found to be

$$\begin{aligned} S_{t_3; t_1' t_2'} &\equiv \langle 0 | a_{\text{out},3}(t_3) a_{\text{in},1}^\dagger(t_1') a_{\text{in},2}^\dagger(t_2') | 0 \rangle \\ &= i\sqrt{\kappa_{1e}\kappa_{2e}\kappa_{3e}} \langle 0 | \hat{T}[a_3(t_3) a_1^\dagger(t_1') a_2^\dagger(t_2')] | 0 \rangle \\ &= i\sqrt{\kappa_{1e}\kappa_{2e}\kappa_{3e}} \left(\langle 0 | a_3(t_3) a_1^\dagger(t_1') a_2^\dagger(t_2') | 0 \rangle \theta(t_3 - t_1') \theta(t_1' - t_2') + \langle 0 | a_3(t_3) a_2^\dagger(t_2') a_1^\dagger(t_1') | 0 \rangle \theta(t_3 - t_2') \theta(t_2' - t_1') \right). \end{aligned} \quad (11)$$

We introduce $|mnr\rangle$ to denote the state with m , n , and r photons in mode a_1 , a_2 , and a_3 , respectively. One key property of the χ^2 trimodal system is that $\{|100\rangle\}$, $\{|010\rangle\}$, and $\{|110\rangle, |001\rangle\}$ form three closed subspaces of the effective Hamiltonian of 1. Based on this property, we proceed to compute Eq. 11:

$$\begin{aligned} &\langle 0 | a_3(t_3) a_1^\dagger(t_1') a_2^\dagger(t_2') | 0 \rangle \\ &= \langle 000 | a_3(t_3) (|001\rangle \langle 001| + |110\rangle \langle 110|) a_1^\dagger(t_1') | 010\rangle \langle 010 | a_2^\dagger(t_2') | 000 \rangle \\ &= \left(\langle 001 | e^{-iH_{\text{eff}}t_3} | 001 \rangle \langle 001 | e^{iH_{\text{eff}}t_1'} | 110 \rangle + \langle 001 | e^{-iH_{\text{eff}}t_3} | 110 \rangle \langle 110 | e^{iH_{\text{eff}}t_1'} | 110 \rangle \right) e^{-i\alpha_2(t_1' - t_2')} \\ &= \frac{g}{\sqrt{\Delta\alpha^2 + 4g^2}} e^{-i\alpha_2(t_1' - t_2')} (e^{i\lambda_2(t_1' - t_3)} - e^{i\lambda_1(t_1' - t_3)}), \end{aligned} \quad (12)$$

where $\Delta\alpha = \alpha_1 + \alpha_2 - \alpha_3$ and $\lambda_{1,2} = \frac{1}{2}(\alpha_1 + \alpha_2 + \alpha_3) \pm \frac{1}{2}\sqrt{\Delta\alpha^2 + 4g^2}$ are the eigenvalues of H_{eff} in the subspace spanned by $|110\rangle$ and $|001\rangle$, i.e.,

$$\begin{bmatrix} \alpha_1 + \alpha_2 & g \\ g & \alpha_3 \end{bmatrix}. \quad (13)$$

The result of $\langle 0|a_3(t_3)a_2^\dagger(t'_2)a_1^\dagger(t'_1)|0\rangle$ is obtained by exchanging the subscripts in Eq. 12. Finally, the momentum-space S -matrix, $S_{p_3;k_1k_2} \equiv \mathcal{F}\{S_{t_3;t'_1t'_2}\}$, is given by

$$S_{p_3;k_1k_2} \equiv i\sqrt{\kappa_{1e}\kappa_{2e}\kappa_{3e}}G(p_3;k_1,k_2) = -ig\frac{\sqrt{\kappa_{1e}\kappa_{2e}\kappa_{3e}}}{\sqrt{2\pi}}\frac{(k_1+k_2-\alpha_1-\alpha_2)}{(k_1-\alpha_1)(k_2-\alpha_2)(k_1+k_2-\lambda_1)(k_1+k_2-\lambda_2)}\delta(p_3-k_1-k_2), \quad (14)$$

where $G(p_3;k_1,k_2)$ is the momentum-space Green's function.

For the degenerate case, i.e., a_1 and a_2 modes are the same mode, the matrix form of H_{eff} in the subspace spanned by $|110\rangle$ (i.e., $|20\rangle$) and $|001\rangle$ is given by

$$\begin{bmatrix} 2\alpha_1 & \sqrt{2}g \\ \sqrt{2}g & \alpha_3 \end{bmatrix}. \quad (15)$$

After a similar derivation, we obtain

$$S_{p_3;k_1k_2} = -2ig\frac{\sqrt{\kappa_{1e}^2\kappa_{3e}}}{\sqrt{2\pi}}\frac{(k_1+k_2-2\alpha_1)}{(k_1-\alpha_1)(k_2-\alpha_1)(k_1+k_2-\lambda'_1)(k_1+k_2-\lambda'_2)}\delta(p_3-k_1-k_2), \quad (16)$$

where $\lambda'_{1,2} = \frac{1}{2}(2\alpha_1+\alpha_3) \pm \frac{1}{2}\sqrt{(2\alpha_1-\alpha_3)^2+8g^2}$ are the eigenvalues of the matrix of 15. It is worth pointing out that $\lambda_{1,2}$ ($\lambda'_{1,2}$) are functions of the trimodal coupling coefficient g , and thus Eqs. 14 and 16 are non-perturbation result in terms of g , contributed by all virtual processes. These processes involving creation and annihilation of virtual photons will be revealed using the Feynman diagram approach in Section III.

The reverse process of one-to-two-photon transport has an S -matrix

$$S_{t'_1t'_2;t_3} \equiv \langle 0|a_{\text{out},1}(t'_1)a_{\text{out},2}(t'_2)a_{\text{in},3}^\dagger(t_3)|0\rangle, \quad (17)$$

whose Fourier transform satisfies

$$S_{k_1k_2;p_3} \equiv \mathcal{F}\{S_{t'_1t'_2;t_3}\} = S_{p_3;k_1k_2}. \quad (18)$$

C. Two-to-two-photon transport

Last, we consider the process of transport of two a_1 and a_2 photons to two a_1 and a_2 photons, without conversion to a_3 photons (Fig. 1d). We again start from the time-domain S -matrix

$$\begin{aligned} S_{t_1t_2;t'_1t'_2} &\equiv \langle 0|a_{\text{out},1}(t_1)a_{\text{out},2}(t_2)a_{\text{in},1}^\dagger(t'_1)a_{\text{in},2}^\dagger(t'_2)|0\rangle \\ &= \delta(t_1-t'_1)\delta(t_2-t'_2) - \kappa_{1e}\langle 0|\hat{T}[a_1(t_1)a_1^\dagger(t'_1)]|0\rangle\delta(t_2-t'_2) - \kappa_{2e}\langle 0|\hat{T}[a_2(t_2)a_2^\dagger(t'_2)]|0\rangle\delta(t_1-t'_1) \\ &\quad + \kappa_{1e}\kappa_{2e}\langle 0|\hat{T}[a_1(t_1)a_1(t_2)a_1^\dagger(t'_1)a_2^\dagger(t'_2)]|0\rangle. \end{aligned} \quad (19)$$

The second and third terms are the single-photon Green's function which have been calculated (see Eq. 7). The last term is new and involves six different time orderings,

$$\begin{aligned} \langle 0|\hat{T}[a_2(t_2)a_1(t_1)a_1^\dagger(t'_1)a_2^\dagger(t'_2)]|0\rangle &= \langle 0|a_2(t_2)a_1(t_1)a_1^\dagger(t'_1)a_2^\dagger(t'_2)|0\rangle\theta(t_2-t_1)\theta(t_1-t'_1)\theta(t'_1-t_2) \\ &\quad + \langle 0|a_2(t_2)a_1(t_1)a_2^\dagger(t'_2)a_1^\dagger(t'_1)|0\rangle\theta(t_2-t_1)\theta(t_1-t'_2)\theta(t'_2-t'_1) \\ &\quad + \langle 0|a_1(t_1)a_1^\dagger(t'_1)a_2(t_2)a_2^\dagger(t'_2)|0\rangle\theta(t_1-t'_1)\theta(t'_1-t_2)\theta(t_2-t'_2) \\ &\quad + \langle 0|a_1(t_1)a_2(t_2)a_2^\dagger(t'_2)a_1^\dagger(t'_1)|0\rangle\theta(t_1-t_2)\theta(t_2-t'_2)\theta(t'_2-t_1) \\ &\quad + \langle 0|a_1(t_1)a_2(t_2)a_1^\dagger(t'_1)a_2^\dagger(t'_2)|0\rangle\theta(t_1-t_2)\theta(t_2-t'_1)\theta(t'_1-t'_2) \\ &\quad + \langle 0|a_2(t_2)a_2^\dagger(t'_2)a_1(t_1)a_1^\dagger(t'_1)|0\rangle\theta(t_2-t'_2)\theta(t'_2-t_1)\theta(t_1-t'_1). \end{aligned} \quad (20)$$

We first calculate $\langle 0 | a_2(t_2) a_1(t_1) a_1^\dagger(t'_1) a_2^\dagger(t'_2) | 0 \rangle$:

$$\begin{aligned}
& \langle 0 | a_2(t_2) a_1(t_1) a_1^\dagger(t'_1) a_2^\dagger(t'_2) | 0 \rangle \\
&= \langle 000 | a_2(t_2) | 010 \rangle \langle 010 | a_1(t_1) (|110\rangle \langle 110| + |001\rangle \langle 001|) a_1^\dagger(t'_1) | 010 \rangle \langle 010 | a_2^\dagger(t'_2) | 000 \rangle \\
&= e^{i\alpha_2(-t_2+t'_2+t_1-t'_1)} \left(\langle 110 | e^{-iH_{\text{eff}}t_1} | 110 \rangle \langle 110 | e^{iH_{\text{eff}}t'_1} | 110 \rangle + \langle 110 | e^{-iH_{\text{eff}}t_1} | 001 \rangle \langle 001 | e^{iH_{\text{eff}}t'_1} | 110 \rangle \right) \\
&= e^{i\alpha_2(-t_2+t'_2+t_1-t'_1)} \left[\left(\frac{1}{2} - \frac{1}{2} \frac{\Delta\alpha}{\sqrt{\Delta\alpha^2 + 4g^2}} \right) e^{-i\lambda_1(t_1-t'_1)} + \left(\frac{1}{2} + \frac{1}{2} \frac{\Delta\alpha}{\sqrt{\Delta\alpha^2 + 4g^2}} \right) e^{-i\lambda_2(t_1-t'_1)} \right].
\end{aligned} \tag{21}$$

Similarly, the second and third terms in Eq. 20 are found to be

$$\langle 0 | a_2(t_2) a_1(t_1) a_2^\dagger(t'_2) a_1^\dagger(t'_1) | 0 \rangle = e^{i\alpha_2(t_1-t_2)} e^{i\alpha_1(t'_1-t'_2)} \left[\left(\frac{1}{2} - \frac{1}{2} \frac{\Delta\alpha}{\sqrt{\Delta\alpha^2 + 4g^2}} \right) e^{-i\lambda_1(t_1-t'_2)} + \left(\frac{1}{2} + \frac{1}{2} \frac{\Delta\alpha}{\sqrt{\Delta\alpha^2 + 4g^2}} \right) e^{-i\lambda_2(t_1-t'_2)} \right], \tag{22}$$

$$\langle 0 | a_1(t_1) a_1^\dagger(t'_1) a_2(t_2) a_2^\dagger(t'_2) | 0 \rangle = e^{i\alpha_1(t'_1-t_1)} e^{i\alpha_2(t'_2-t_2)}. \tag{23}$$

The rest three terms in Eq. 20 are obtained by simply exchanging the indices 1 and 2 in Eqs. 21-23.

Finally, by Fourier transform of Eq. 20, we obtain the momentum-space Green's function

$$G(p_1, p_2; k_1, k_2) = -\frac{1}{(k_1 - \alpha_1)(k_2 - \alpha_2)} \delta(p_1 - k_1) \delta(p_2 - k_2) + M(p_1, p_2, k_1, k_2) \delta(p_1 + p_2 - k_1 - k_2), \tag{24}$$

where

$$M(p_1, p_2, k_1, k_2) = -\frac{ig^2}{2\pi} \frac{k_1 + k_2 - \alpha_1 - \alpha_2}{(k_1 - \alpha_1)(k_2 - \alpha_2)(p_1 - \alpha_1)(p_2 - \alpha_2)(k_1 + k_2 - \lambda_1)(k_1 + k_2 - \lambda_2)}, \tag{25}$$

and the momentum-space S -matrix

$$S_{p_1 p_2; k_1 k_2} = t_{k_1} t_{k_2} \delta(p_1 - k_1) \delta(p_2 - k_2) + \kappa_{1e} \kappa_{2e} M(p_1, p_2, k_1, k_2) \delta(p_1 + p_2 - k_1 - k_2). \tag{26}$$

For the case of degenerate a_1 and a_2 , after a similar derivation, we have

$$G(p_1, p_2; k_1, k_2) = -\frac{1}{(k_1 - \alpha_1)(k_2 - \alpha_1)} [\delta(p_1 - k_1) \delta(p_2 - k_2) + \delta(p_1 - k_2) \delta(p_2 - k_1)] + M(p_1, p_2, k_1, k_2) \delta(p_1 + p_2 - k_1 - k_2) \tag{27}$$

and

$$S_{p_1 p_2; k_1 k_2} = t_{k_1} t_{k_2} [\delta(p_1 - k_1) \delta(p_2 - k_2) + \delta(p_1 - k_2) \delta(p_2 - k_1)] + \kappa_{1e}^2 M(p_1, p_2, k_1, k_2) \delta(p_1 + p_2 - k_1 - k_2), \tag{28}$$

where

$$M(p_1, p_2, k_1, k_2) = -\frac{2ig^2}{\pi} \frac{k_1 + k_2 - 2\alpha_1}{(k_1 - \alpha_1)(k_2 - \alpha_1)(p_1 - \alpha_1)(p_2 - \alpha_1)(k_1 + k_2 - \lambda'_1)(k_1 + k_2 - \lambda'_2)}. \tag{29}$$

Eqs. 26 and 28 show that the S -matrix of two-to-two-photon transport consists of an interaction-free component, which is the product of two single-photon transmission coefficients, and an interaction-mediated component. The total transport amplitude is given by the superposition of the two components, representing the quantum interference between the two pathways. This leads to profound consequences of the photon-photon interaction via the waveguide-coupled nonlinear optical cavities and applications in quantum information science (see Section IV). The interaction-mediated component

was also interpreted as the two-photon bound state previously [10].

III. FEYNMAN DIAGRAM APPROACH

In this section, we introduce a perturbation method based on Feynman diagrams to calculate the momentum-space Green's function and S -matrix. The perturbation method, suited for weak nonlinear systems with $g/\kappa_j < 1$, reveals the relevant physical processes con-

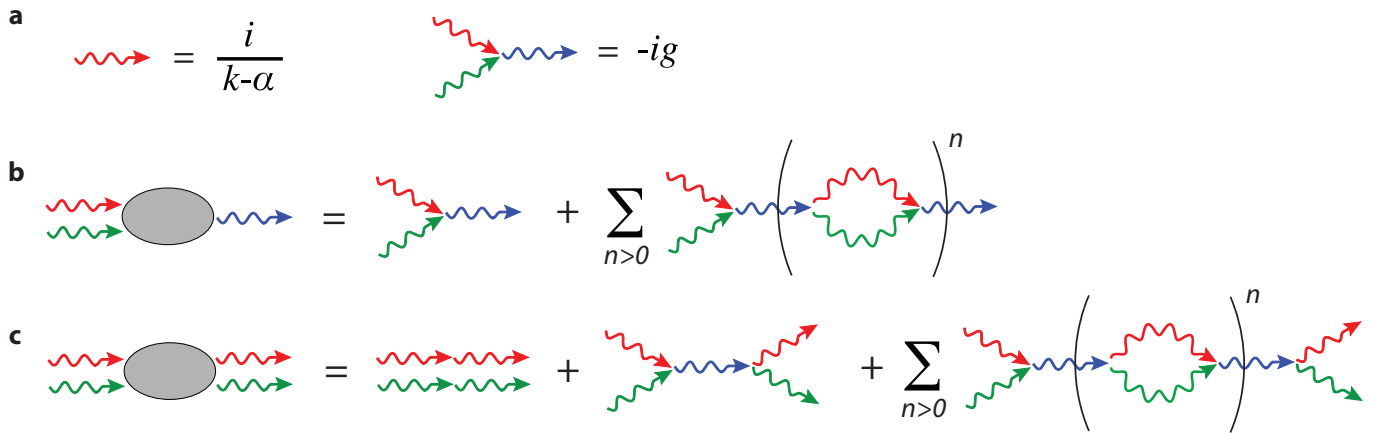


FIG. 2. **a**. Feynman diagram rules for the propagator and vertex. Red, green, and blue lines corresponds to a_1 , a_2 , and a_3 mode photons, respectively. **b** and **c**. Feynman diagrams contributing to the Green's function of two-to-one-photon transport (**b**) and two-to-two-photon transport (**c**). The part enclosed by the parenthesis is repeated by n times.

tributing to the few-photon transport amplitude. It is also mathematically simplified, especially when only the leading order Feynman diagrams are of interest, compared to the previous method where careful cancellation of divergence is needed when performing the Fourier transform of the time-domain Green's function involving the Heaviside step function. The Feynman diagram rules here resemble those developed in quantum field theory (see, e.g., Ref. [28]). In essence, the n -operator Green's function is calculated using all connected Feynman diagrams with n external points, which are constructed from basic elements including "propagator" and "vertex". The propagator is the two-point free-particle Green's function and the vertex corresponds to the bare interaction term of the Hamiltonian. For the Hamiltonian of 1, the Feynman diagram rules are given as follows:

- Propagator: $\frac{i}{k-\alpha}$,
- Vertex: $-ig$,
- Impose energy conservation at each vertex: $\frac{1}{\sqrt{2\pi}}\delta(\sum k - \sum p)$,
- Integrate undetermined momentum: $\int dk \int dp$.

- Multiply the symmetry factor: $m!$ for m propagators of the same mode connecting two vertices or connecting a vertex with external points.

The Feynman diagrams corresponding to the propagator and vertex are shown in Fig. 2a. A few differences from the Feynman diagram rules for field operators in quantum field theory are worth noting. Here, because the equation of motion for the cavity mode operator is a linear differential equation, the propagator, given by Eq. 9, is linearly dependent on the momentum. Further, because the effective Hamiltonian of the open quantum system already includes loss terms, i.e., $i\kappa_j$, the propagator does not diverge at the real resonance frequency, avoiding the addition of an infinitesimal imaginary term in the propagator for performing the momentum integrals.

The three- and four-point momentum-space Green's functions related to Eqs. 11 and 20 can be calculated using the Feynman diagrams shown in Fig. 2b and c, respectively. These Feynman diagrams also illustrates the physical processes, involving creation and annihilation of virtual photons, that contribute to the photon transport amplitude. After computation of each Feynman diagram according to the rules above, the three-point Green's function is found to be

$$G(p_3; k_1, k_2) = -\frac{g}{\sqrt{2\pi}} \frac{1}{(k_1 - \alpha_1)(k_2 - \alpha_2)(p_3 - \alpha_3)} \sum_{n=0}^{\infty} \left(\frac{g^2}{(p_3 - \alpha_1 - \alpha_2)(p_3 - \alpha_3)} \right)^n \delta(p_3 - k_1 - k_2), \quad (30)$$

where the term of $n = 0$ corresponds to the first diagram on the right hand side in Fig. 2b and each term of $n > 0$

corresponds to the diagram with n repeated part in the parenthesis. The four-point Green's function is found to be

$$\begin{aligned}
& G(p_1, p_2; k_1, k_2) \\
&= -\frac{1}{(k_1 - \alpha_1)(k_2 - \alpha_2)} \delta(p_1 - k_1) \delta(p_2 - k_2) \\
&\quad - \frac{ig^2}{2\pi} \frac{1}{(k_1 - \alpha_1)(k_2 - \alpha_2)(p_1 - \alpha_1)(p_2 - \alpha_2)(k_1 + k_2 - \alpha_3)} \sum_{n=0}^{\infty} \left(\frac{g^2}{(k_1 + k_2 - \alpha_1 - \alpha_2)(k_1 + k_2 - \alpha_3)} \right)^n \delta(p_1 + p_2 - k_1 - k_2),
\end{aligned} \tag{31}$$

where the first term corresponds to the first diagram on the right hand side in Fig. 2c, the term of $n = 0$ corresponds to the second diagram, and each term of $n > 0$ corresponds to the diagram with n repeated part in the parenthesis. One can confirm that Eqs. 30 and 31 reproduce Eqs. 14 and 24, respectively, after performing the summation. As an example of applying the Feyn-

man diagram rules, we explicitly show the calculation of the $n = 1$ diagram in Fig. 2b. Higher order diagrams are essentially multiple repetition of the component in the parenthesis of this basic diagram. The formula corresponding to this diagram, following the Feynman diagram rules from left to right, is given by

$$\begin{aligned}
& \frac{i}{k_1 - \alpha_1} \frac{i}{k_2 - \alpha_2} \frac{-ig}{\sqrt{2\pi}} \int dq_3 \delta(q_3 - k_1 - k_2) \frac{i}{q_3 - \alpha_3} \frac{-ig}{\sqrt{2\pi}} \int dq_1 dq_2 \delta(q_1 + q_2 - q_3) \frac{i}{q_1 - \alpha_1} \frac{i}{q_2 - \alpha_2} \frac{-ig}{\sqrt{2\pi}} \delta(q_1 + q_2 - p_3) \frac{i}{p_3 - \alpha_3} \\
&= -\frac{g}{\sqrt{2\pi}} \delta(p_3 - k_1 - k_2) \frac{1}{(k_1 - \alpha_1)(k_2 - \alpha_2)(p_3 - \alpha_3)} \frac{-g^2}{2\pi i} \int dq_1 dq_2 \delta(q_1 + q_2 - p_3) \frac{1}{q_1 - \alpha_1} \frac{1}{q_2 - \alpha_2} \frac{1}{p_3 - \alpha_3} \\
&= -\frac{g}{\sqrt{2\pi}} \delta(p_3 - k_1 - k_2) \frac{1}{(k_1 - \alpha_1)(k_2 - \alpha_2)(p_3 - \alpha_3)} \frac{g^2}{(p_3 - \alpha_1 - \alpha_2)(p_3 - \alpha_3)},
\end{aligned} \tag{32}$$

which yields the $n = 1$ term in Eq. 30.

We note Eqs. 30 and 31 are power series expansion in terms of $(g/\kappa)^2$, where κ is the shorthand notation for κ_j or their sum, for input and output photons in resonant with the cavity modes, i.e., $k_j, p_j \approx \omega_j$, and a frequency-matched cavity ($\omega_1 + \omega_2 \approx \omega_3$). As a result, only leading order Feynman diagrams are needed for weak nonlinear optical cavities, i.e., $(g/\kappa)^2 < 1$, which significantly simplifies the calculation. The computation here is also divergence free, in contrast to the method used in the previous Section which encounters divergences during Fourier transform of the time-domain Green's function and thus requires careful cancellations [14]

IV. OBSERVATIONAL EFFECTS OF FEW-PHOTON TRANSPORT

In this Section, we discuss several observational effects associated with the few-photon transport via a waveguide-coupled $\chi^{(2)}$ cavity. Throughout this Section, we consider input photons in a weak coherent state, which are commonly used for single-photon level experiments.

A. Single-photon down-conversion

We first consider the down-conversion process of a_3 photons to a_1 and a_2 photons. The input weak coherent state of monochromatic a_3 photons can be written as

$$|\psi_{\text{in}}\rangle = |0\rangle + \alpha |1_t\rangle + \frac{\alpha^2}{\sqrt{2}} |1_t 1_t\rangle + O(\alpha^3), \tag{33}$$

where α is the amplitude of the coherent state and $|1_t\rangle = |1\rangle e^{-ikt}$ represents a monochromatic single-photon state with momentum k in the time domain. Note $|1_t\rangle \neq |t\rangle$. We are interested in the second-order correlation function of the output a_1 and a_2 photons:

$$\begin{aligned}
& g^{(2)}(\tau) \\
&= \frac{\langle \psi_{\text{in}} | a_{\text{out},1}^\dagger(t) a_{\text{out},2}^\dagger(t+\tau) a_{\text{out},2}(t+\tau) a_{\text{out},1}(t) | \psi_{\text{in}} \rangle}{\langle \psi_{\text{in}} | a_{\text{out},1}^\dagger(t) a_{\text{out},1}(t) | \psi_{\text{in}} \rangle \langle \psi_{\text{in}} | a_{\text{out},2}^\dagger(t) a_{\text{out},2}(t) | \psi_{\text{in}} \rangle},
\end{aligned} \tag{34}$$

which can be calculated using the momentum-space S -matrix. To do so, we first perform a Fourier transform of $|\psi_{\text{in}}\rangle$:

$$\mathcal{F}\{|\psi_{\text{in}}\rangle\} = \int \frac{dt}{\sqrt{2\pi}} e^{ik't} |1\rangle e^{-ikt} = \sqrt{2\pi} |1\rangle \delta(k' - k). \tag{35}$$

Thus we define Fourier-transformed monochromatic single-photon state to be $\sqrt{2\pi} |1_k\rangle$. Keeping the leading order term in $|\psi_{\text{in}}\rangle$, we have

$$\begin{aligned}
& \langle \psi_{\text{in}} | a_{\text{out},1}^\dagger(t) a_{\text{out},2}^\dagger(t+\tau) a_{\text{out},2}(t+\tau) a_{\text{out},1}(t) | \psi_{\text{in}} \rangle \\
&= |\alpha|^2 \langle 1_t | a_{\text{out},1}^\dagger(t) a_{\text{out},2}^\dagger(t+\tau) a_{\text{out},2}(t+\tau) a_{\text{out},1}(t) | 1_t \rangle \\
&= |\alpha|^2 \langle 1_t | a_{\text{out},1}^\dagger(t) a_{\text{out},2}^\dagger(t+\tau) | 0 \rangle \langle 0 | a_{\text{out},2}(t+\tau) a_{\text{out},1}(t) | 1_t \rangle \\
&= \frac{|\alpha|^2}{2\pi} \int dp_1 dp_2 \langle 1_k | a_{\text{out},1}^\dagger(p_1) a_{\text{out},2}^\dagger(p_2) | 0 \rangle e^{ip_1 t + ip_2(t+\tau)} \\
&\quad \times \int d\tilde{p}_1 d\tilde{p}_2 \langle 0 | a_{\text{out},2}(\tilde{p}_2) a_{\text{out},1}(\tilde{p}_1) | 1_k \rangle e^{-i\tilde{p}_1 t - i\tilde{p}_2(t+\tau)} \\
&= \frac{|\alpha|^2}{2\pi} \int dp_1 dp_2 S_{p_1 p_2; k}^* e^{ip_1 t + ip_2(t+\tau)} \\
&\quad \times \int d\tilde{p}_1 d\tilde{p}_2 S_{\tilde{p}_1 \tilde{p}_2; k} e^{-i\tilde{p}_1 t - i\tilde{p}_2(t+\tau)} \\
&= \begin{cases} \frac{|\alpha|^2 g^2 \kappa_{1e} \kappa_{2e} \kappa_{3e}}{|(k-\lambda_1)(k-\lambda_2)|^2} e^{-\kappa_2 \tau}, \tau > 0, \\ \frac{|\alpha|^2 g^2 \kappa_{1e} \kappa_{2e} \kappa_{3e}}{|(k-\lambda_1)(k-\lambda_2)|^2} e^{\kappa_1 \tau}, \tau < 0, \end{cases}
\end{aligned} \tag{36}$$

where $S_{p_1 p_2; k}$ is given by Eq. 18, and

$$\begin{aligned}
& \langle \psi_{\text{in}} | a_{\text{out},1}^\dagger(t) a_{\text{out},1}(t) | \psi_{\text{in}} \rangle \\
&= |\alpha|^2 \langle 1_t | a_{\text{out},1}^\dagger(t) a_{\text{out},1}(t) | 1_t \rangle \\
&= |\alpha|^2 \int dp_1 d\tilde{p}_1 \langle 1_k | a_{\text{out},1}^\dagger(p_1) a_{\text{out},1}(\tilde{p}_1) | 1_k \rangle e^{ip_1 t - i\tilde{p}_1 t} \\
&= |\alpha|^2 \int dp_1 d\tilde{p}_1 \langle 1_k | a_{\text{out},1}^\dagger(p_1) \left(\int dp_2 |p_2\rangle \langle p_2| + \int dp_{2i} |p_{2i}\rangle \langle p_{2i}| \right) a_{\text{out},1}(\tilde{p}_1) | 1_k \rangle e^{ip_1 t - i\tilde{p}_1 t} \\
&= |\alpha|^2 \left(\int dp_1 d\tilde{p}_1 dp_2 S_{p_1 p_2; k} S_{\tilde{p}_1 p_2; k}^* + \frac{\kappa_{2i}}{\kappa_{2e}} \int dp_1 d\tilde{p}_1 dp_{2i} S_{p_1 p_{2i}; k} S_{\tilde{p}_1 p_{2i}; k}^* \right) e^{ip_1 t - i\tilde{p}_1 t} \\
&= |\alpha|^2 \frac{\kappa_2}{\kappa_{2e}} \int dp_1 d\tilde{p}_1 dp_2 S_{p_1 p_2; k} S_{\tilde{p}_1 p_2; k}^* e^{ip_1 t - i\tilde{p}_1 t} \\
&= |\alpha|^2 \frac{\kappa_{1e}}{\kappa_1} \frac{g^2 (\kappa_1 + \kappa_2) \kappa_{3e}}{|(k-\lambda_1)(k-\lambda_2)|^2},
\end{aligned} \tag{37}$$

where $|p_{2i}\rangle$ represents the state of a_2 photons in the intrinsic loss channel. Because the states in the waveguide and the intrinsic loss channel combined form a complete Hilbert space of the leaked photons from the cavity, we have the identity

$$\int dp_2 |p_2\rangle \langle p_2| + \int dp_{2i} |p_{2i}\rangle \langle p_{2i}| = I. \tag{38}$$

In other words, $\langle \psi_{\text{in}} | a_{\text{out},1}^\dagger(t) a_{\text{out},1}(t) | \psi_{\text{in}} \rangle$ measures the total a_1 photon flux, regardless of the place of a_2 photons, which could either be in the waveguide or the intrinsic loss channel. Thus, we have to insert Eq. 38 into Eq. 37. We have also used the fact that the S -matrix involving $|p_{2i}\rangle$ will be proportional to $\sqrt{\kappa_{2i}}$, by replacing $\sqrt{\kappa_{2e}}$ in Eq. 14. Exchanging subscripts 1 and 2 in Eq. 37 yields the result of $\langle \psi_{\text{in}} | a_{\text{out},2}^\dagger(t) a_{\text{out},2}(t) | \psi_{\text{in}} \rangle$. The intra-cavity photon-pair generation rate is inferred from Eq. 37 to be

$$R = |\alpha|^2 \frac{g^2 (\kappa_1 + \kappa_2) \kappa_{3e}}{|(k-\lambda_1)(k-\lambda_2)|^2}. \tag{39}$$

Finally, we have

$$g^{(2)}(\tau) = \frac{|(k-\lambda_1)(k-\lambda_2)|^2}{2|\alpha|^2 g^2 (\kappa_1 + \kappa_2) \kappa_{3e}} \frac{2\kappa_1 \kappa_2}{\kappa_1 + \kappa_2} \times \begin{cases} e^{-\kappa_2 \tau}, \tau > 0, \\ e^{\kappa_1 \tau}, \tau < 0, \end{cases} \tag{40}$$

and in the limit $g \ll \kappa_{1,2,3}$,

$$\begin{aligned}
g^{(2)}(\tau) &\approx \frac{((k-\omega_1-\omega_2)^2 + (\frac{\kappa_1+\kappa_2}{2})^2) ((k-\omega_3)^2 + (\frac{\kappa_3}{2})^2)}{2|\alpha|^2 g^2 (\kappa_1 + \kappa_2) \kappa_{3e}} \\
&\quad \times \frac{2\kappa_1 \kappa_2}{\kappa_1 + \kappa_2} \times \begin{cases} e^{-\kappa_2 \tau}, \tau > 0, \\ e^{\kappa_1 \tau}, \tau < 0. \end{cases}
\end{aligned} \tag{41}$$

Interestingly, Eq. 41 is identical to the result of spontaneous parametric down-conversion derived via a semiclassical approach by assuming non-depleted classical pumps and using Gaussian moment factoring theorem [16, 29].

B. Photon blockade

Next, we consider transport of a_1 photons via a cavity with degenerate a_1 and a_2 modes. For input of a_1 photons in this case, there will be probability of up-conversion to output a_3 photons; however, we focus on the process without such up-conversion, which could be separated apart from the up-converted a_3 photons because a_1 and a_3 photons are disparate in frequency. Assuming monochromatic input a_1 photons in a weak coherent state given by Eq. 33, we compute the second-order self-correlation function of the transported a_1 photons:

$$g^{(2)}(\tau) = \frac{\langle \psi_{\text{in}} | a_{\text{out},1}^\dagger(t) a_{\text{out},1}^\dagger(t+\tau) a_{\text{out},1}(t+\tau) a_{\text{out},1}(t) | \psi_{\text{in}} \rangle}{\langle \psi_{\text{in}} | a_{\text{out},1}^\dagger(t) a_{\text{out},1}(t) | \psi_{\text{in}} \rangle \langle \psi_{\text{in}} | a_{\text{out},1}^\dagger(t) a_{\text{out},1}(t) | \psi_{\text{in}} \rangle}. \quad (42)$$

By keeping the leading order terms in $|\psi_{\text{in}}\rangle$, we have

$$\begin{aligned} & \langle \psi_{\text{in}} | a_{\text{out},1}^\dagger(t) a_{\text{out},1}(t) | \psi_{\text{in}} \rangle \\ &= |\alpha|^2 \langle 1_t | a_{\text{out},1}^\dagger(t) a_{\text{out},1}(t) | 1_t \rangle \\ &= |\alpha|^2 \langle 1_t | a_{\text{out},1}^\dagger(t) | 0 \rangle \langle 0 | a_{\text{out},1}(t) | 1_t \rangle \\ &= |\alpha|^2 \int dp e^{ipt} \langle 1_k | a_{\text{out},1}^\dagger(p) | 0 \rangle \int d\tilde{p} e^{-i\tilde{p}t} \langle 0 | a_{\text{out},1}(\tilde{p}) | 1_k \rangle \\ &= |\alpha|^2 \int dp e^{ipt} S_{p;k}^* \int d\tilde{p} e^{-i\tilde{p}t} S_{\tilde{p};k} \\ &= |\alpha|^2 |t_k|^2 \end{aligned} \quad (43)$$

and

$$\begin{aligned} & \langle \psi_{\text{in}} | a_{\text{out},1}^\dagger(t) a_{\text{out},1}^\dagger(t+\tau) a_{\text{out},1}(t+\tau) a_{\text{out},1}(t) | \psi_{\text{in}} \rangle \\ &= \frac{|\alpha|^4}{2} \langle 1_t 1_{t+\tau} | a_{\text{out},1}^\dagger(t) a_{\text{out},1}^\dagger(t+\tau) a_{\text{out},1}(t+\tau) a_{\text{out},1}(t) | 1_t 1_{t+\tau} \rangle \\ &= \frac{|\alpha|^4}{2} \int dp_1 dp_2 \langle 1_k 1_k | a_{\text{out},1}^\dagger(p_1) a_{\text{out},1}^\dagger(p_2) | 0 \rangle e^{ip_1 t + ip_2(t+\tau)} \\ & \quad \times \int d\tilde{p}_1 d\tilde{p}_2 \langle 0 | a_{\text{out},1}(\tilde{p}_2) a_{\text{out},1}(\tilde{p}_1) | 1_k 1_k \rangle e^{-i\tilde{p}_1 t - i\tilde{p}_2(t+\tau)} \\ &= \frac{|\alpha|^4}{4} \int dp_1 dp_2 S_{p_1 p_2; k k}^* e^{ip_1 t + ip_2(t+\tau)} \\ & \quad \times \int d\tilde{p}_1 d\tilde{p}_2 S_{\tilde{p}_1 \tilde{p}_2; k k} e^{-i\tilde{p}_1 t - i\tilde{p}_2(t+\tau)} \\ &= |\alpha|^4 |t_k^2 + T(k, \tau)|^2, \end{aligned} \quad (44)$$

where the S -matrix is given by Eq. 28 and

$$T(k, \tau) = -\frac{2g^2 \kappa_{1e}^2}{(2k - \lambda'_1)(2k - \lambda'_2)(k - \alpha_1)^2} e^{-i|\tau|(\alpha_1 - k)}. \quad (45)$$

Note the additional factor of 1/2 in the third equality of Eq. 44 comes from the definition of Fock state $|1_k 1_k\rangle =$

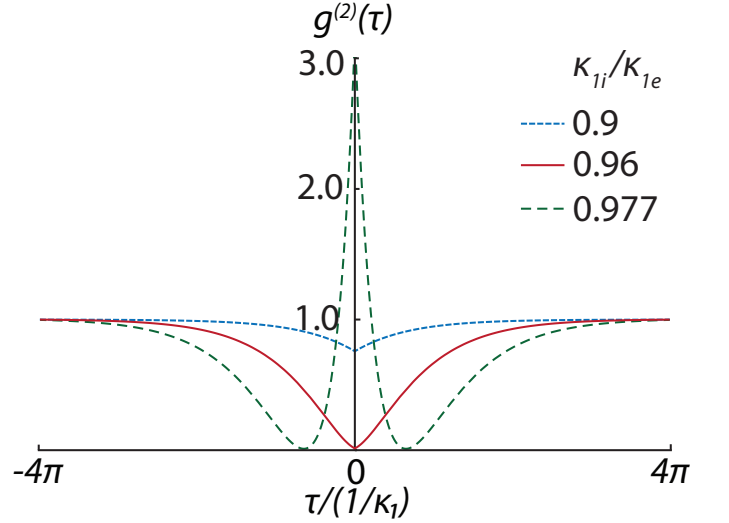


FIG. 3. $g^{(2)}(\tau)$ for various κ_{1e}/κ_{1i} , given $k = \omega_1$, $g/\kappa_{1i} = 0.02$, $\kappa_{3i} = 2\kappa_{1i}$, $\kappa_{3e} = 0.1\kappa_{1i}$.

$|2_k\rangle = \frac{1}{\sqrt{2}} a_{\text{in}}^{\dagger 2}(k) |0\rangle$. Finally, we have

$$g^{(2)}(\tau) = \frac{|t_k^2 + T(k, \tau)|^2}{|t_k^2|^2}. \quad (46)$$

This result is remarkable in that even when $|T(k, \tau)|$ is small, which is the case for practical $\chi^{(2)}$ nonlinear optical cavities with $g/\kappa \ll 1$, highly nonclassical correlations of transported photons, i.e., $g^{(2)}(\tau) \neq 1$, could be achieved by making $|t_k^2|$ close to $|T(k, \tau)|$. This is due to the quantum interference between the interaction-free and interaction-mediated amplitudes of the two-photon transport, as indicated by the S -matrix (Eq. 26), especially when the two amplitudes are compatible. To illustrate this more explicitly, for the one-port, phase-matched cavity ($2\omega_1 = \omega_3$) and on-resonance input photons ($k = \omega_1$),

$$t_{\omega_1}^2 = \left(\frac{\kappa_{1i} - \kappa_{1e}}{\kappa_{1i} + \kappa_{1e}} \right)^2 \quad (47)$$

and

$$T(\omega_1, 0) = -\frac{8g^2 \kappa_{1e}^2}{\kappa_{1i}^2 (\kappa_{1i} \kappa_{3i} / 2 + 2g^2)}. \quad (48)$$

Thus, by making κ_{1i} and κ_{1e} such that $t_{\omega_1}^2 \approx -T(\omega_1, 0)$, one obtains $g^{(2)}(0) \approx 0$, which indicates the photon blockade. Remarkably, this can be achieved even for $g/\kappa_{1,3} \ll 1$, if $\kappa_{1i} \approx \kappa_{1e}$, i.e., close to the critical coupling between the cavity and waveguide. We note the minus sign of $T(\omega_1, 0)$ is important in cancellation with $t_{\omega_1}^2$; intuitively, this is because during the interaction-mediated process the state $|20\rangle$ undergoes a Rabi flip with the virtual state $|01\rangle$ and back again, which yields a Berry phase of π .

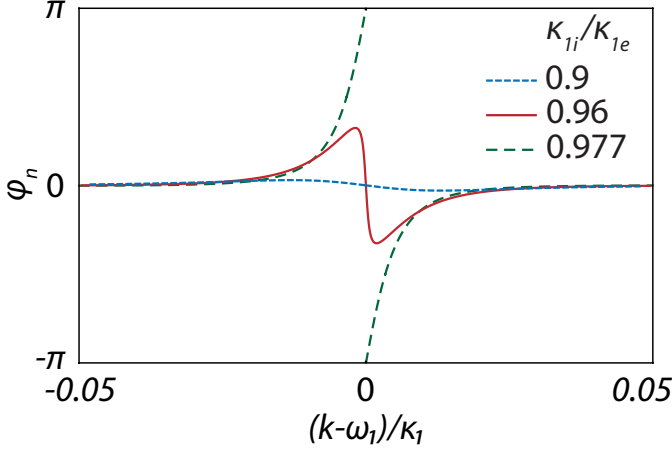


FIG. 4. Nonlinear phase shift for various κ_{1e}/κ_{1i} , given $g/\kappa_{1i} = 0.02$, $\kappa_{3i} = 2\kappa_{1i}$, $\kappa_{3e} = 0.1\kappa_{1i}$.

Moreover, the statistical properties of the output a_1 photons can be altered, e.g., from anti-bunching to bunching ($g^{(2)}(0) > g^{(2)}(\tau)$), by controlling t_k^2 via κ_{1e} or κ_{1i} . This is shown in Fig. 3. For these plots, we have used experimentally achievable device parameters of a state-of-the-art $\chi^{(2)}$ nonlinear photonic platform with g/κ_{1i} in the range of a few percent [22]. The correlation functions of finite wavepackets can also be calculated using the S -matrix, taking into account of the spectral distribution of the wavepacket. The result is included in Appendix B, which shows the averaging effect on the nonclassical correlation due to the finite spectral width of the wavepacket. However, this is not surprising because the cavity-based mechanism is expected to work only for wavepackets with spectral width much smaller than the cavity linewidth.

C. Nonlinear phase shift

The photon-photon interaction in the $\chi^{(2)}$ cavity also induces a nonlinear phase shift of the transported photons. To compute the nonlinear phase shift, we point out the numerator of the second-order correlation function (Eq. 42) actually gives the norm of the time-domain wavefunction of the transported two photons (see Appendix A). Thus, the wavefunction of the transported two photons can be written as

$$\langle t, t + \tau | \psi_{\text{out}} \rangle = e^{-ik(2t+\tau)} (t_k^2 + T(k, \tau)). \quad (49)$$

The wavefunction of two photons without the interaction is

$$\langle t, t + \tau | \psi_{\text{out}}^{(0)} \rangle = e^{-ik(2t+\tau)} t_k^2. \quad (50)$$

The nonlinear phase shift due to the photon-photon interaction thus is

$$\begin{aligned} \varphi_n &\equiv \text{Arg} [\langle t, t + \tau | \psi_{\text{out}} \rangle] - \text{Arg} [\langle t, t + \tau | \psi_{\text{out}}^{(0)} \rangle] \\ &= \text{Arg} \left[1 + \frac{T(k, \tau)}{t_k^2} \right]. \end{aligned} \quad (51)$$

By making $|t_k^2| \approx |T(k, \tau)|$, large nonlinear phase shift can be achieved, which is possible even for the weak coupling regime $g \ll \kappa_1$. Such nonlinear phase shift is a key enabler for quantum nondemolition measurement of photons [23] and conditional quantum logic gates [24, 30].

Fig. 4 shows the calculated nonlinear phase shift (for $\tau = 0$) using experimentally achievable parameters of a state-of-the-art $\chi^{(2)}$ nonlinear photonic platform [22]. It is seen that large and even π -nonlinear phase shift can be achieved in practical devices. Actually, π -nonlinear phase shift is always achieved at $k = \omega_1$ as long as $t_{\omega_1}^2 < -T(\omega_1, 0)$.

D. Two-mode nonclassical correlation

In Sections IV B and IV C, we considered a cavity with degenerate a_1 and a_2 modes. Here, we consider a cavity with non-degenerate a_1 and a_2 modes which satisfy the frequency-matching condition $\omega_1 + \omega_2 \approx \omega_3$ and show nonclassical two-mode correlations could be generated. We assume now the input state to be the product of two weak coherent states in modes a_1 and a_2 ,

$$\begin{aligned} |\psi_{\text{in}}\rangle &= |\alpha\rangle_1 |\beta\rangle_2 \\ &= \left(|0\rangle + \alpha |1_t\rangle_1 + \frac{\alpha^2}{\sqrt{2}} |1_t 1_t\rangle_1 + O(\alpha^3) \right) \\ &\quad \times \left(|0\rangle + \beta |1_t\rangle_2 + \frac{\beta^2}{\sqrt{2}} |1_t 1_t\rangle_2 + O(\beta^3) \right). \end{aligned} \quad (52)$$

The two-mode and single-mode correlations are, respectively,

$$\begin{aligned} G_{12}(\tau) &= \langle \psi_{\text{in}} | a_{\text{out},1}^\dagger(t) a_{\text{out},2}^\dagger(t+\tau) a_{\text{out},2}(t+\tau) a_{\text{out},1}(t) | \psi_{\text{in}} \rangle \\ &= |\alpha\beta|^2 \int dp_1 dp_2 \langle 1_{k_1} 1_{k_2} | a_{\text{out},1}^\dagger(p_1) a_{\text{out},2}^\dagger(p_2) | 0 \rangle e^{ip_1 t + ip_2(t+\tau)} \\ &\quad \times \int d\tilde{p}_1 d\tilde{p}_2 \langle 0 | a_{\text{out},2}(\tilde{p}_2) a_{\text{out},1}(\tilde{p}_1) | 1_{k_1} 1_{k_2} \rangle e^{-i\tilde{p}_1 t - i\tilde{p}_2(t+\tau)} \\ &= |\alpha\beta|^2 \int dp_1 dp_2 S_{p_1 p_2; k_1 k_2}^* e^{ip_1 t + ip_2(t+\tau)} \\ &\quad \times \int d\tilde{p}_1 d\tilde{p}_2 S_{\tilde{p}_1 \tilde{p}_2; k_1 k_2} e^{-i\tilde{p}_1 t - i\tilde{p}_2(t+\tau)} \\ &= |\alpha\beta|^2 |t_{k_1} t_{k_2} + \tilde{T}(k_1, k_2, \tau)|^2, \end{aligned} \quad (53)$$

where the S -matrix is given by Eq. 26 and

$$\begin{aligned} & \tilde{T}(k_1, k_2, \tau) \\ &= \begin{cases} -\frac{g^2 \kappa_1 e^{\kappa_2 e}}{(k_1+k_2-\lambda_1)(k_1+k_2-\lambda_2)(k_1-\alpha_1)(k_2-\alpha_2)} e^{-i\tau(\alpha_2-k_2)}, \tau > 0, \\ -\frac{g^2 \kappa_1 e^{\kappa_2 e}}{(k_1+k_2-\lambda_1)(k_1+k_2-\lambda_2)(k_1-\alpha_1)(k_2-\alpha_2)} e^{i\tau(\alpha_1-k_1)}, \tau < 0, \end{cases} \end{aligned} \quad (54)$$

and

$$\begin{aligned} & G_{11}(\tau) \\ &= \langle \psi_{\text{in}} | a_{\text{out},1}^\dagger(t) a_{\text{out},1}^\dagger(t+\tau) a_{\text{out},1}(t+\tau) a_{\text{out},1}(t) | \psi_{\text{in}} \rangle \\ &= \frac{|\alpha|^4}{2} \int dp_1 dp_2 \langle 1_{k_1} 1_{k_1} | a_{\text{out},1}^\dagger(p_1) a_{\text{out},1}^\dagger(p_2) | 0 \rangle e^{ip_1 t + ip_2(t+\tau)} \\ & \quad \times \int d\tilde{p}_1 d\tilde{p}_2 \langle 0 | a_{\text{out},1}(\tilde{p}_1) a_{\text{out},1}(\tilde{p}_2) | 1_{k_1} 1_{k_1} \rangle e^{-i\tilde{p}_2 t - i\tilde{p}_1(t+\tau)} \\ &= \frac{|\alpha|^4}{4} \int dp_1 dp_2 2t_{k_1}^* t_{k_1}^* \delta(p_1 - k_1) \delta(p_2 - k_1) e^{ip_1 t + ip_2(t+\tau)} \\ & \quad \times \int d\tilde{p}_1 d\tilde{p}_2 2t_{k_1} t_{k_1} \delta(p_1 - k_1) \delta(p_2 - k_1) e^{-i\tilde{p}_2 t - i\tilde{p}_1(t+\tau)} \\ &= |\alpha|^4 |t_{k_1}|^4, \end{aligned} \quad (55)$$

and similarly,

$$G_{22}(\tau) = |\beta|^4 |t_{k_2}|^4. \quad (56)$$

In Eq. 55, we have used the fact that the transport of two a_1 photons via a non-degenerate cavity is interaction-free because $2\omega_1 \neq \omega_3$.

To measure the nonclassicality of the two-mode correlation, we define

$$\zeta(\tau) \equiv \frac{G_{12}(\tau)}{\sqrt{G_{11}(\tau)G_{22}(\tau)}} = \left| 1 + \frac{\tilde{T}(k_1, k_2, \tau)}{t_{k_1} t_{k_2}} \right|^2. \quad (57)$$

$\zeta(\tau) > 1$ leads to violation of the Cauchy-Schwartz in-

equality and indicates nonclassical two-mode correlations [31]. Given the similarity of Eq. 57 and Eq. B6, it is obvious that $\zeta(\tau) > 1$ can be achieved when $|t_{k_1} t_{k_2}|$ is sufficiently smaller than $|\tilde{T}(k_1, k_2, \tau)|$.

V. CONCLUSION

In summary, we have theoretically studied few-photon transport via a waveguide-coupled, multimode $\chi^{(2)}$ optical cavity. We used both non-perturbative method and a new perturbation method based on Feynman diagrams to compute the S -matrix associated with the few-photon transport. The Feynman diagram approach provides physical insight into the transport process and is mathematically convenient. The S -matrix shows that the two-photon transport involves quantum interference between linear transmission and interaction-mediated transport. This effect leads to rather unexpected result that strong quantum correlations could be realized in weak non-linear systems by matching the linear transmission coefficient with the interaction-mediated amplitude. We numerically showed several pronounced quantum optical effects, including photon blockade and π -conditional phase shift, could be achieved in state-of-the-art non-linear quantum photonic platforms, which might have a significant impact on using these systems for quantum information science applications.

Appendix A: The wavefunction of transported photons

Here we prove the second-order correlation actually gives the norm of the output two-photon wavefunction.

$$\begin{aligned} & \langle \psi_{\text{in}} | a_{\text{out}}^\dagger(t) a_{\text{out}}^\dagger(t+\tau) a_{\text{out}}(t+\tau) a_{\text{out}}(t) | \psi_{\text{in}} \rangle \\ &= \frac{1}{(2\pi)^2} \int dp_1 dp_2 dp_3 dp_4 e^{i(p_1 t + p_2(t+\tau) - p_3(t+\tau) - p_4 t)} \langle \psi_{\text{in}} | \hat{S}^\dagger \hat{S} a_{\text{out}}^\dagger(p_1) \hat{S}^\dagger \hat{S} a_{\text{out}}^\dagger(p_2) \hat{S}^\dagger \hat{S} a_{\text{out}}(p_3) \hat{S}^\dagger \hat{S} a_{\text{out}}(p_4) \hat{S}^\dagger \hat{S} | \psi_{\text{in}} \rangle \\ &= \frac{1}{(2\pi)^2} \int dp_1 dp_2 dp_3 dp_4 e^{i(p_1 t + p_2(t+\tau) - p_3(t+\tau) - p_4 t)} \langle \psi_{\text{out}} | a_{\text{in}}^\dagger(p_1) a_{\text{in}}^\dagger(p_2) a_{\text{in}}(p_3) a_{\text{in}}(p_4) | \psi_{\text{out}} \rangle \\ &= \frac{1}{(2\pi)^2} \int dp_1 dp_2 dp_3 dp_4 e^{i(p_1 t + p_2(t+\tau) - p_3(t+\tau) - p_4 t)} \langle \psi_{\text{out}} | a_{\text{in}}^\dagger(p_1) a_{\text{in}}^\dagger(p_2) | 0 \rangle \langle 0 | a_{\text{in}}(p_3) a_{\text{in}}(p_4) | \psi_{\text{out}} \rangle \\ &= \frac{1}{(2\pi)^2} \int dp_1 dp_2 e^{i(p_1 t + p_2(t+\tau))} \langle p_1, p_2 | \psi_{\text{out}} \rangle^* \int dp_3 dp_4 e^{-i(p_3(t+\tau) + p_4 t)} \langle p_3, p_4 | \psi_{\text{out}} \rangle \\ &= |\langle t, t+\tau | \psi_{\text{out}} \rangle|^2 \end{aligned} \quad (A1)$$

where $|t, t+\tau\rangle$ represents the state of two photons at time t and $t+\tau$, respectively, and thus the end result gives the time-domain wavefunction of the output two photons. We have used \hat{S} to represent the operator cor-

responding to the S -matrix defined in the momentum space, which satisfies the unitary condition $\hat{S}^\dagger \hat{S} = \hat{I}$. We have also assumed the input/output states contain up to two photons, which is consistent with Eq. 33.

Appendix B: Correlation functions for photon wavepackets

We consider the input state being a photon wavepacket, i.e., $|\psi_{\text{in}}\rangle = \exp(\alpha a^\dagger - \alpha^* a)|0\rangle$, where $a =$

$\int dk f(k)a_k$ and $f(k)$ is the spectral distribution centered around k_0 and satisfying $\int |f(k)|^2 dk = 1$. The first- and second-order correlation functions for the photon wavepacket are given by

$$\begin{aligned}
& \langle \psi_{\text{in}} | a_{\text{out},1}^\dagger(t) a_{\text{out},1}(t) | \psi_{\text{in}} \rangle \\
&= |\alpha|^2 \int dk_1 d\tilde{k}_1 f(k_1) f(\tilde{k}_1) \langle 1_{k_1} | a_{\text{out},1}^\dagger(t) a_{\text{out},1}(t) | 1_{\tilde{k}_1} \rangle \\
&= |\alpha|^2 \int dk_1 d\tilde{k}_1 f(k_1) f(\tilde{k}_1) \langle 1_{k_1} | a_{\text{out},1}^\dagger(p_1) a_{\text{out},1}(\tilde{p}_1) | 1_{\tilde{k}_1} \rangle e^{i(p_1 - \tilde{p}_1)t} \\
&= |\alpha|^2 \int dk_1 dp_1 f(k_1) e^{ip_1 t} S_{p_1 k_1}^* \int d\tilde{k}_1 d\tilde{p}_1 f(\tilde{k}_1) e^{-i\tilde{p}_1 t} S_{\tilde{p}_1 \tilde{k}_1} \\
&= |\alpha|^2 \int dk_1 f(k_1) e^{ik_1 t} t_{k_1}^* \int d\tilde{k}_1 f(\tilde{k}_1) e^{-i\tilde{k}_1 t} t_{\tilde{k}_1} \\
&= |\alpha|^2 |\tilde{t}(k_0, t)|^2,
\end{aligned} \tag{B1}$$

where $\tilde{t}(k_0, t) = \int dk_1 f(k_1) e^{-ik_1 t} t_{k_1}$, and

$$\begin{aligned}
& \langle \psi_{\text{in}} | a_{\text{out},1}^\dagger(t) a_{\text{out},1}^\dagger(t + \tau) a_{\text{out},1}(t + \tau) a_{\text{out},1}(t) | \psi_{\text{in}} \rangle \\
&= \frac{|\alpha|^4}{2} \int dp_1 dp_2 dk_1 dk_2 \langle 1_{k_1} 1_{k_2} | a_{\text{out},1}^\dagger(p_1) a_{\text{out},1}^\dagger(p_2) | 0 \rangle e^{ip_1 t + ip_2(t + \tau)} f(k_1) f(k_2) \\
&\quad \times \int d\tilde{p}_1 d\tilde{p}_2 d\tilde{k}_1 d\tilde{k}_2 \langle 0 | a_{\text{out},1}(\tilde{p}_2) a_{\text{out},1}(\tilde{p}_1) | 1_{\tilde{k}_1} 1_{\tilde{k}_2} \rangle e^{-i\tilde{p}_1 t - i\tilde{p}_2(t + \tau)} f(\tilde{k}_1) f(\tilde{k}_2) \\
&= \frac{|\alpha|^4}{4} \int dp_1 dp_2 S_{p_1 p_2; k_1 k_1}^* e^{ip_1 t + ip_2(t + \tau)} f(k_1) f(k_2) \\
&\quad \times \int d\tilde{p}_1 d\tilde{p}_2 S_{\tilde{p}_1 \tilde{p}_2; \tilde{k}_1 \tilde{k}_2} e^{-i\tilde{p}_1 t - i\tilde{p}_2(t + \tau)} f(\tilde{k}_1) f(\tilde{k}_2) \\
&= |\alpha|^4 |\tilde{t}(k_0, t) \tilde{t}(k_0, t + \tau) + \tilde{T}(k_0, t, \tau)|^2,
\end{aligned} \tag{B2}$$

where

$$\tilde{T}(k_0, t, \tau) = \frac{1}{2} \int dk_1 dk_2 dp_1 \kappa_{1e}^2 M(p_1, k_1 + k_2 - p, k_1, k_2) e^{-ip_1 t - i(k_1 + k_2 - p_1)(t + \tau)} f(k_1) f(k_2). \tag{B3}$$

To illustrate the effect of finite spectral width of wavepackets, we consider a spectral distribution of $f(k) = \sqrt{\frac{2}{\pi\gamma}} \frac{\gamma^2}{(k - k_0)^2 + \gamma^2}$ which leads to

$$\tilde{t}(k_0, t) = \begin{cases} \sqrt{2\pi\gamma} [e^{-i(k_0 - i\gamma)t} (1 - \frac{i\kappa_{1e}}{k_0 - i\gamma - \alpha_1}) - e^{-i\alpha_1 t} \frac{2\gamma\kappa_{1e}}{(\alpha_1 - k_0)^2 + \gamma^2}], & t > 0, \\ \sqrt{2\pi\gamma} e^{-i(k_0 + i\gamma)t} (1 - \frac{i\kappa_{1e}}{k_0 + i\gamma - \alpha_1}), & t < 0 \end{cases} \tag{B4}$$

and

$$\tilde{T}(k_0, t = 0, \tau) = -\frac{4\pi g^2 \kappa_{1e}^2 \gamma}{(k_0 + i\gamma - \alpha_1)^2 (2k_0 + 2i\gamma - \lambda_1') (2k_0 + 2i\gamma - \lambda_2')} \times \begin{cases} e^{-i\alpha_1 \tau}, & \tau > 0, \\ e^{-2i(k_0 + i\gamma)\tau + i\alpha_1 \tau}, & \tau < 0. \end{cases} \tag{B5}$$

We assume the wavepacket to be sufficiently long and thus ignore the temporal wavepacket shape. The normalized second-order correlation function thus is given

by, setting $t = 0$,

$$g^{(2)}(\tau) = \frac{|\tilde{t}(k_0, 0) \tilde{t}(k_0, \tau) + \tilde{T}(k_0, 0, \tau)|^2}{|\tilde{t}(k_0, 0)|^2 |\tilde{t}(k_0, \tau)|^2}. \tag{B6}$$

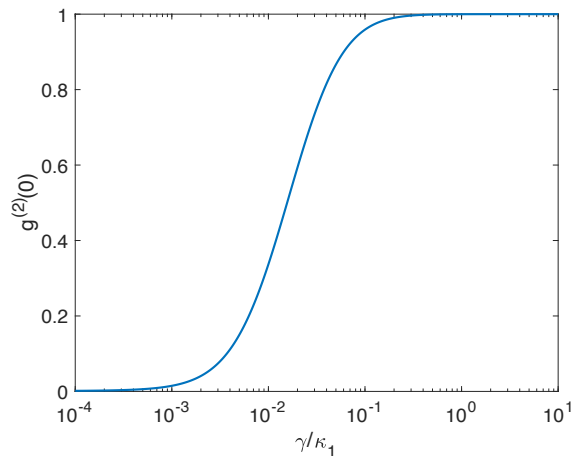


FIG. 5. $g^{(2)}(0)$ as a function of wavepacket width γ . Other parameters used in the calculation are $k_0 = \omega_1$, $g/\kappa_{1i} = 0.02$, $\kappa_{1i}/\kappa_{1e} = 1.04$, $\kappa_{3i} = 2\kappa_{1i}$, $\kappa_{3e} = 0.1\kappa_{1i}$.

We plot $g^{(2)}(0)$ as a function of γ in Fig. 5 for a parameter set which yields $g^{(2)}(0) = 0$ for $\gamma \rightarrow 0$, i.e., the continuous-wave limit. The averaging effect is observed due to the spectral span of the photon wavepacket, leading to $g^{(2)}(0)$ increasing from 0 to 1. However, $g^{(2)}(0)$ remains sufficiently small for $\gamma \leq 10^{-2}\kappa_1$.

-
- [1] TG Tiecke, Jeffrey Douglas Thompson, Nathalie Pulmones de Leon, LR Liu, Vladan Vuletić, and Mikhail D Lukin, “Nanophotonic quantum phase switch with a single atom,” *Nature* **508**, 241–244 (2014).
- [2] Itay Shomroni, Serge Rosenblum, Yulia Lovsky, Orel Bechler, Gabriel Guendelman, and Barak Dayan, “All-optical routing of single photons by a one-atom switch controlled by a single photon,” *Science* **345**, 903–906 (2014).
- [3] Jürgen Volz, Michael Scheucher, Christian Junge, and Arno Rauschenbeutel, “Nonlinear π phase shift for single fibre-guided photons interacting with a single resonator-enhanced atom,” *Nature Photonics* **8**, 965–970 (2014).
- [4] Alisa Javadi, I Söllner, Marta Arcari, S Lindskov Hansen, Leonardo Midolo, Sahand Mahmoodian, G Kiršanskė, Tommaso Pregnolato, EH Lee, JD Song, *et al.*, “Single-photon non-linear optics with a quantum dot in a waveguide,” *Nature communications* **6**, 1–5 (2015).
- [5] Alp Sipahigil, Ruffin E Evans, Denis D Sukachev, Michael J Burek, Johannes Borregaard, Mihir K Bhaskar, Christian T Nguyen, Jose L Pacheco, Haig A Atikian, Charles Meuwly, *et al.*, “An integrated diamond nanophotonics platform for quantum-optical networks,” *Science* **354**, 847–850 (2016).
- [6] Mohammad Mirhosseini, Eunjong Kim, Vinicius S Ferreira, Mahmoud Kalaei, Alp Sipahigil, Andrew J Keller, and Oskar Painter, “Superconducting metamaterials for waveguide quantum electrodynamics,” *Nature communications* **9**, 1–7 (2018).
- [7] Bharath Kannan, Max J Ruckriegel, Daniel L Campbell, Anton Frisk Kockum, Jochen Braumüller, David K Kim, Morten Kjaergaard, Philip Krantz, Alexander Melville, Bethany M Niedzielski, *et al.*, “Waveguide quantum electrodynamics with superconducting artificial giant atoms,” *Nature* **583**, 775–779 (2020).
- [8] Christoph Simon, “Towards a global quantum network,” *Nature Photonics* **11**, 678–680 (2017).
- [9] Darrick E Chang, Anders S Sørensen, Eugene A Demler, and Mikhail D Lukin, “A single-photon transistor using nanoscale surface plasmons,” *Nature physics* **3**, 807–812 (2007).
- [10] Jung-Tsung Shen and Shanhui Fan, “Strongly correlated multiparticle transport in one dimension through a quantum impurity,” *Physical Review A* **76**, 062709 (2007).
- [11] Jie-Qiao Liao, CK Law, *et al.*, “Correlated two-photon transport in a one-dimensional waveguide side-coupled to a nonlinear cavity,” *Physical Review A* **82**, 053836 (2010).
- [12] Huaixiu Zheng, Daniel J Gauthier, and Harold U Baranger, “Waveguide qed: Many-body bound-state effects in coherent and fock-state scattering from a two-level system,” *Physical Review A* **82**, 063816 (2010).
- [13] Eden Rephaeli and Shanhui Fan, “Few-photon single-atom cavity qed with input-output formalism in fock space,” *IEEE Journal of Selected Topics in Quantum Electronics* **18**, 1754–1762 (2012).
- [14] Shanshan Xu and Shanhui Fan, “Input-output formalism for few-photon transport: A systematic treatment beyond two photons,” *Physical Review A* **91**, 043845 (2015).
- [15] David P Lake, Matthew Mitchell, Harishankar Jayakumar, Laís Fujii Dos Santos, Davor Curic, and Paul E Barclay, “Efficient telecom to visible wavelength conversion in doubly resonant gallium phosphide microdisks,” *Applied Physics Letters* **108**, 031109 (2016).
- [16] Xiang Guo, Chang-ling Zou, Carsten Schuck, Hojoong Jung, Risheng Cheng, and Hong X Tang, “Parametric down-conversion photon-pair source on a nanophotonic chip,” *Light: Science & Applications* **6**, e16249–e16249 (2017).
- [17] Rui Luo, Yang He, Hanxiao Liang, Mingxiao Li, and Qiang Lin, “Highly tunable efficient second-harmonic generation in a lithium niobate nanophotonic waveguide,” *Optica* **5**, 1006–1011 (2018).
- [18] Lin Chang, Andreas Boes, Paolo Pintus, Jon D Peters, MJ Kennedy, Xiao-Wen Guo, Nicolas Volet, Su-Peng

- Yu, Scott B Papp, and John E Bowers, “Strong frequency conversion in heterogeneously integrated gaas resonators,” *APL Photonics* **4**, 036103 (2019).
- [19] Mian Zhang, Brandon Buscaino, Cheng Wang, Amirhasan Shams-Ansari, Christian Reimer, Rongrong Zhu, Joseph M Kahn, and Marko Lončar, “Broadband electro-optic frequency comb generation in a lithium niobate microring resonator,” *Nature* **568**, 373–377 (2019).
- [20] Daniil M Lukin, Constantin Dory, Melissa A Guidry, Ki Youl Yang, Sattwik Deb Mishra, Rahul Trivedi, Marina Radulaski, Shuo Sun, Dries Vercautse, Geun Ho Ahn, *et al.*, “4h-silicon-carbide-on-insulator for integrated quantum and nonlinear photonics,” *Nature Photonics* **14**, 330–334 (2020).
- [21] Xiyuan Lu, Gregory Moille, Ashutosh Rao, Daron A Westly, and Kartik Srinivasan, “Efficient photoinduced second-harmonic generation in silicon nitride photonics,” *Nature Photonics* **15**, 131–136 (2021).
- [22] Mengdi Zhao and Kejie Fang, “Ingap quantum nanophotonic integrated circuits with 1.5% second-order nonlinearity,” arXiv preprint arXiv:2105.12705 (2021).
- [23] Keyu Xia, Mattias Johnsson, Peter L Knight, Jason Twamley, *et al.*, “Cavity-free scheme for nondestructive detection of a single optical photon,” *Physical review letters* **116**, 023601 (2016).
- [24] Nathan K Langford, Sven Ramelow, Robert Prevedel, William J Munro, Gerard J Milburn, and Anton Zeilinger, “Efficient quantum computing using coherent photon conversion,” *Nature* **478**, 360 (2011).
- [25] Nicolas Sangouard, Bruno Sanguinetti, Noé Curtz, Nicolas Gisin, Rob Thew, and Hugo Zbinden, “Faithful entanglement swapping based on sum-frequency generation,” *Physical review letters* **106**, 120403 (2011).
- [26] Daniel F Walls and Gerard J Milburn, *Quantum optics* (Springer Science & Business Media, 2007).
- [27] Shanhui Fan, Şükrü Ekin Kocabaş, and Jung-Tsung Shen, “Input-output formalism for few-photon transport in one-dimensional nanophotonic waveguides coupled to a qubit,” *Physical Review A* **82**, 063821 (2010).
- [28] Michael E Peskin, *An introduction to quantum field theory* (CRC press, 2018).
- [29] Christoph Clausen, Félix Bussières, Alexey Tiranov, Harald Herrmann, Christine Silberhorn, Wolfgang Sohler, Mikael Afzelius, and Nicolas Gisin, “A source of polarization-entangled photon pairs interfacing quantum memories with telecom photons,” *New Journal of Physics* **16**, 093058 (2014).
- [30] Quentin A Turchette, Christina J Hood, Wolfgang Lange, HJKH Mabuchi, and H Jeffrey Kimble, “Measurement of conditional phase shifts for quantum logic,” *Physical Review Letters* **75**, 4710 (1995).
- [31] Leonard Mandel and Emil Wolf, *Optical coherence and quantum optics* (Cambridge university press, 1995).

Acknowledgements

This work is supported by US National Science Foundation under Grant No. DMS 18-39177.